Protocol

High-Speed Two-Photon Calcium Imaging of Neuronal Population Activity Using Acousto-Optic Deflectors

Benjamin F. Grewe and Fritjof Helmchen

Two-photon calcium imaging of neuronal populations allows optical measurements of spiking activity in living animals. However, laser-scanning microscopes with galvanometric scan mirrors are too slow to capture population activity on a millisecond timescale. This protocol describes a two-photon microscope that is based on two-dimensional laser scanning with acousto-optic deflectors (AODs), enabling high-speed in vivo recording of neuronal population activity at temporal resolutions of several hundred hertz. The detailed construction plan of the AOD-based microscope is accompanied by equally detailed optimization procedures. We also introduce a novel random-access pattern scanning (RAPS) technique for high-speed in vivo measurements of neuronal population activity. AOD-based RAPS can measure calcium transients in neocortical neuronal populations, revealing spike trains with near-millisecond precision. The current limitations of the AOD-based microscope are discussed, and we provide an outlook of its future applications.

MATERIALS

It is essential that you consult the appropriate Material Safety Data Sheets and your institution's Environmental Health and Safety Office for proper handling of equipment and hazardous materials used in this protocol.

RECIPE: Please see the end of this protocol for recipes indicated by <R>. Additional recipes can be found online at http://cshprotocols.cshlp.org/site/recipes.

Reagents

Agarose, type III-A (1%, prepared in normal rat Ringer [NRR] solution; Sigma-Aldrich)

Calcium indicator dye, membrane-permeable (e.g., acetoxymethyl [AM] form of Oregon Green 1,2-bis-(2-aminophenoxy)ethane-*N*,*N*,*N*′,*N*′-tetra-acetic acid (BAPTA)-1 [OGB-1; Invitrogen])

Mice, wild-type

Normal rat Ringer's solution <R>

Sulforhodamine 101 (SR101; e.g., from Sigma-Aldrich)

Sulforhodamine is used for specific counterstaining of cortical astrocytes (Nimmerjahn et al. 2004). See ***In Vivo Labeling of Cortical Astrocytes with Sulforhodamine 101 (SR101)*** *(Nimmerjahn and Helmchen 2012).*

Urethane

Equipment

Anaesthesia-monitoring equipment

See ***In Vivo Two-Photon Calcium Imaging Using Multicell Bolus Loading*** *(Garaschuk and Konnerth 2010).*

Adapted from *Imaging in Neuroscience* (ed. Helmchen and Konnerth). CSHL Press, Cold Spring Harbor, NY, USA, 2011.

Cite this protocol as *Cold Spring Harb Protoc*; doi:10.1101/pdb.prot081778

Beads, fluorescent (≤500 nm)

Microscope, two-photon, acousto-optic deflector (AOD)-based

See Imaging Setup in the Discussion for a detailed list of required parts.

Surgical equipment

*See **In Vivo Two-Photon Calcium Imaging Using Multicell Bolus Loading** (Garaschuk and Konnerth 2010).*

METHOD

Microscope Setup

For a detailed list of parts and considerations in assembly, see Imaging Setup in the Discussion. To set up the optical light path of the microscope, use a "backward" approach: (1) Mount the microscope objective, (2) install the tube and scan lenses, (3) mount the AOD scanners and the dispersion compensation unit (DCU), and (4) proceed with the beam alignment. For direct viewing of the samples, mount a binocular in the beam path (Fig. 1A).

1. Set up the laser, the shutter, the Pockels cell, and the variable beam expander.
2. Fix the motorized *x*–*y* stage on the optical table.
3. Mount the X95 column with two base plates attached on the *x*–*y* stage.
4. Using a clamping carrier, mount the linear *z* stage onto the 95× column.

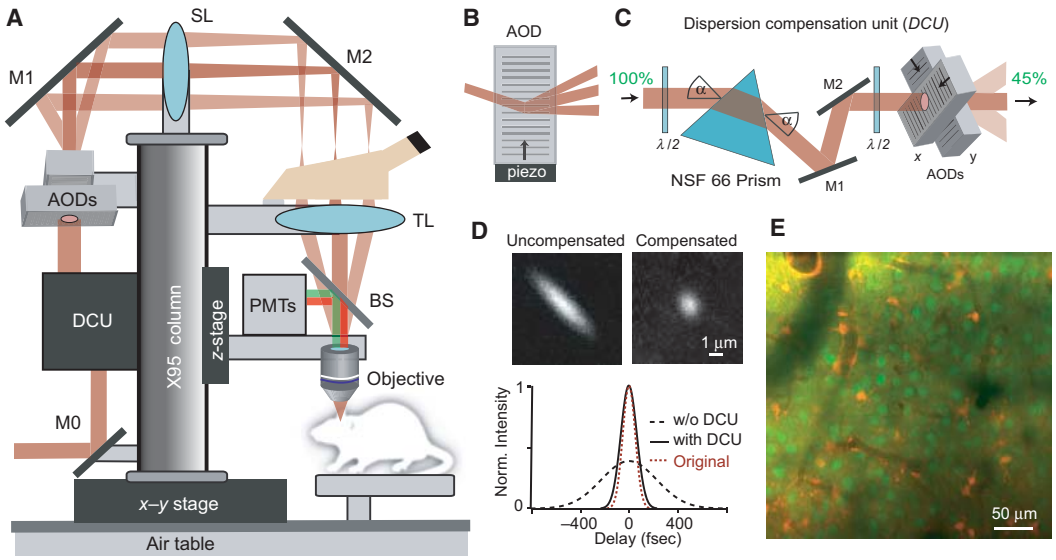

FIGURE 1. Microscope setup for AOD-based high-speed calcium imaging. (*A*) Schematic of the two-photon microscope setup mounted on an air table. A motorized *x*–*y* stage supports movements of the entire microscope over the sample. After the DCU, two orthogonal AODs are used for *x*–*y* scanning. Scan (SL) and tube (TL) lenses provide a large field of view (FOV) (~300 µm) with a 40× objective. BS, beam splitter; M0, M1, M2, mirrors. (*B*) Schematic of laser beam scanning with an AOD crystal. A standing sound wave is produced by a piezoelectric transducer and acts as a diffraction grating. The angle of laser beam deflection is proportional to the piezo-oscillation frequency. (*C*) Schematic of the optical path through the single-prism DCU consisting of two λ/2 plates and a custom prism oriented at 45° to the AOD axes. If an SF11 prism is used, an additional cylindrical telescope (not shown) is required to compensate for beam ellipticity caused by mismatch of the input and output angle at the prism. (*D*) Compensation of spatial and temporal dispersion. (*Top*) Two-photon images of 500-nm fluorescent beads without (*left*) and with (*right*) the DCU. Note that compensation abolishes ellipticity. (*Bottom*) Laser pulse width with and without the DCU. The single-prism DCU nearly restores the original pulse width under the objective. (*E*) Two-photon fluorescence image of neocortical L2/3 cell populations in intact mouse neocortex. Cells were bulk labeled with the calcium indicator OGB-1; astrocytes were counterstained with SR101.

5. Construct a custom objective holder. Attach it to the *z* stage.

   We use a distance of ~20 cm of the optical axis from the column to facilitate the alignment procedures and to provide plenty of space beneath the objective (e.g., for a living animal).

6. Design and construct a fluorescence detection pathway that includes a sliding two-photon beam splitter, the dichroic mirrors, fluorescence filters, and PMTs.

   This system uses two channels but, in principle, more channels can be added.

7. Attach the fluorescence detection unit (from Step 6) to the linear *z* stage directly above the objective.
8. Install the tube lens at the appropriate distance (i.e., f_{TL}) above the objective.
9. Mount the scan lens at the correct distance from the tube lens ($f_{TL} + f_{SL}$) on top of the 95× column.
10. Use a 45° mirror (BB2-E03) to redirect the laser beam (M2 in Fig. 1A).
11. Mount the AODs at the correct distance from the scan lens (f_{SL}) on the opposite side of the column.
12. Use a 45° mirror (BB2-E03) to redirect the laser beam to the AOD scanners (M1 in Fig. 1A).
13. Insert a λ/2-wave plate in a rotation mount. Use a clamping carrier to mount this assembly before the AODs.
14. Mount the prism rotation mount (with the compensation prism) on a clamping carrier.

    Use a custom-built holder to install the compensation prism at an angle of 45° with respect to the AOD axes (Fig. 1C).

15. Attach mirror mounts for two mirrors after the prism that redirect the laser beam to the AODs (M1 and M2 in Fig. 1C).
16. Install a λ/2-wave plate (in a rotation mount) on a clamping carrier in front of the compensation prism.
17. Mount a 45° mirror at the 95× column base to reflect the laser beam into the microscope (M0 in Fig. 1A).
18. Mount two mirrors oriented 90° to each other onto the two linear moving parts of the *x*–*y* motorized stage (i.e., in the *x*- and *y*-directions, respectively; mirrors not shown in Fig. 1A).

    These mirrors are used to steer the fixed input laser beam to the microscope while avoiding laser beam runoff during stage movements.

Alignment and Optimization Procedures

The microscope design is kept relatively simple, with only two key components that must be properly aligned (the AOD scanners and the DCU prism). Given ~45% transmission through these two components, the total transmission efficiency of the entire microscope should not go below ~25% (assuming an 850-nm wavelength and the use of a 40× objective). Because the DCU prism and the AODs form a pair of dispersive elements that provide negative group velocity dispersion, they can be used to compensate for temporal pulse broadening in the light path. Optimal compensation is achieved by adjusting the distance between the DCU prism and the AODs, so that minimal pulse lengths are achieved behind the objective (Fig. 1D). Pulse width can be measured directly with an autocorrelator; alternatively, the obtained fluorescence signal can be maximized (see below). To correct for spatial dispersion, the aim is to obtain a uniformly round focus shape in the field of view (FOV) center with a full-width at half-maximum of ~1 µm. Performance is best evaluated by imaging small (100–500 nm) fluorescent beads (Fig. 1D). Note that optimal compensation of spatial dispersion is only possible in the FOV center and that lateral resolution and beam ellipticity worsen toward the edges and corners of the FOV.

19. Remove the AODs, λ/2-wave plates, and the DCU by removing the clamps from the 95× column.
20. With the help of an iris, adjust the two in-coupling mirrors (from Step 18) that steer the laser beam into the microscope (via M0 in Fig. 1A) to ensure a stable laser beam alignment during stage movements.

21. Use two or more irises to center the beam on all lenses and the objective. Also, center the laser beam on the mirrors (M1 and M2 in Fig. 1A).
22. Remount the AOD scanners.
23. Drive the AODs with the center frequency. Center the laser beam by shifting the AODs laterally with respect to the laser beam.

    See Troubleshooting.

24. Adjust the pitch/yaw platform below the AODs to optimize the incident angle and ensure maximum laser beam diffraction efficiency, as measured using the power meter.
25. Reinstall the DCU. Adjust the incident angle of the laser beam to ~53° for the N-SF11 prism (or ~69° for the N-SF66 prism).
26. Realign the laser beam after the DCU with respect to the AODs.

    A distance of ~35 cm between the AODs and the DCU prism is a good starting point for nearly restoring the original laser pulse width (Fig. 1D). The optimal distance depends on the specific optical components used in the beam path and can be found empirically (see Step 30).

27. Reinstall and adjust the first λ/2-wave plate before the prism to ensure maximum laser beam transmission through the prism, as measured using the power meter.
28. Reinstall the second λ/2-wave plate before the AODs. Turn the polarization to maximize AOD diffraction efficiency, as measured using the power meter.
29. Position small (≤500 nm) round fluorescent beads in the FOV. Adjust the incident angle of the laser beam at the prism to achieve a homogeneous bead resolution (Fig. 1D).

    The laser beam needs to be realigned with respect to the AODs by using the two parallel mirrors of the DCU each time the prism angle is changed.

    See Troubleshooting.

30. To optimize compensation of the temporal dispersion (i.e., to achieve the shortest pulses below the objective), shift the complete DCU parallel to the 95× column until the fluorescence signal is maximal.

    Perform this optimization during AOD scanning. Alternatively, measure the laser pulse width below the objective with an autocorrelator. Realign the laser beam for maximal signal each time after shifting the DCU.

31. During regular maintenance, be sure to check the alignment of the two key components (i.e., the AODs and the DCU prism), which can be adjusted slightly without any major laser beam runoff.

Animal Preparation

*For experimental procedures for animal preparation and dye labeling (bolus loading) of cell populations, see **In Vivo Two-Photon Calcium Imaging Using Multicell Bolus Loading** (Garaschuk and Konnerth 2010). Perform all procedures in accordance with the guidelines, and with the approval, of your local animal facility.*

32. Anesthetize mice, for example, by intraperitoneal administration of urethane (1.2–1.5 g/kg body weight).
33. Perform a craniotomy above the brain region of interest (e.g., the barrel cortex) and carefully remove the dura if needed.
34. Superfuse the exposed cortex with NRR solution.
35. Bolus load neurons in the superficial layers of the cortex in the area under study with a calcium-sensitive fluorescent dye (e.g., OGB-1) (Stosiek et al. 2003).
36. To distinguish neurons from astrocytes, counterstain the latter by application of SR101 to the exposed brain surface for several minutes (Nimmerjahn et al. 2004).
37. To dampen heartbeat- and breathing-induced motion, fill the cranial window with 1% agarose. Cover with a glass coverslip.

38. Place animals under the custom-built AOD two-photon microscope and start two-photon imaging in the frame-scan mode.

Random Access Pattern Scanning of Neuronal Populations

The main advantage of using AOD laser scanners is the possibility to rapidly shift the focal excitation spot between any two positions within the scanning field within only a few microseconds (10 µsec in our setup). Therefore, stained cell populations can be scanned in a "random-access" manner avoiding waste of time on background regions. To optimize dwell times on neuronal somata and to minimize effects of photobleaching and phototoxicity, we devised a random-access pattern scanning (RAPS) modus, in which a small stereotype point pattern is sequentially run on each neuron in the population (Fig. 2A).

39. Search for an area of interest that contains well-stained neurons. Choose an appropriate zoom factor to clearly identify neuronal somata.

    Stained neurons and astrocytes are visualized in the green and red detection channels, respectively.

    See Troubleshooting.

40. Before random-access scanning, acquire a reference image at high spatial resolution using the standard 2D frame scanning mode with the AODs (Fig. 1E).

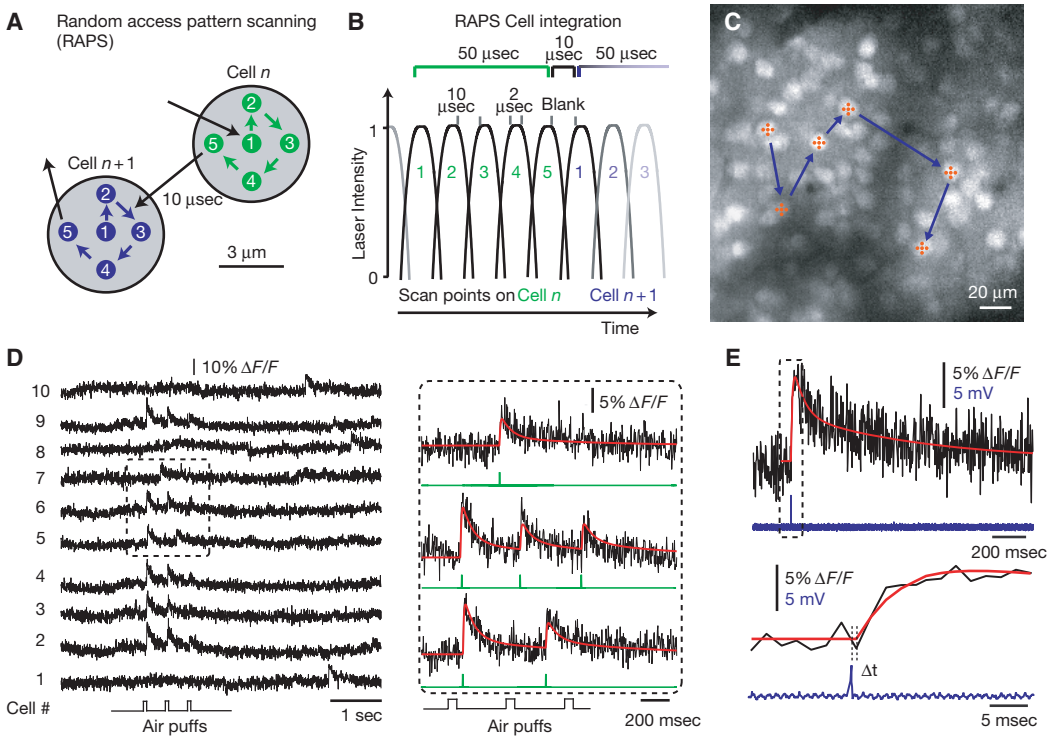

FIGURE 2. High-speed random-access recording of calcium signals in neocortical networks. (*A*) The principle of RAPS is exemplified by a five-point pattern that is sequentially scanned on two cell somata. (*B*) Signal integration protocol for five-point RAPS. Cellular fluorescence signals are integrated over the entire five-point scan periods except for the 10-µsec transition between cells. (*C*) L2/3 neuronal population in mouse barrel cortex labeled with OGB-1 (depth = 210 µm). High-speed imaging using a 314-Hz sampling rate per cell was performed using five-point RAPS on 53 cells manually preselected from a reference image. Five of the RAPS transitions are shown in the image. (*D*) Calcium transients in 10 of the 53 selected L2/3 neurons in response to whisker stimulation by three air puffs at 2.5 Hz (*left*). Close-up of the responses of three cells (as indicated in the box at *left*) to air-puff stimulation (*right*). Model traces (red) are reconstructed by an automated spike detection algorithm. (*E*) Example of a single action-potential-evoked calcium transient (measured at 490 Hz) fitted with a model trace (red) (*top*). A simultaneous in vivo juxtacellular recording reveals the spike eliciting the calcium transient. Expanded plot of the onset of the single action-potential-evoked calcium transient and its temporal relationship to the simultaneously recorded spike (*bottom*). In this case, the difference (Δt) between actual spike time and the spike time estimate obtained from the onset fit (red) was 0.7 msec.

Cite this protocol as *Cold Spring Harb Protoc*; doi:10.1101/pdb.prot081778

41. Choose your stereotype scan pattern, defined by the number of points (n = 1–9; we mostly used five points) and the geometrical arrangement (e.g., as a cross or a circle).

42. Define the random-access pattern scanning pathway by manually selecting neuronal somata from the previously acquired reference image. From the positions of the selected cells (and the selected pattern), a user-defined list of all scan positions is created and sent to the AOD driving electronics.

    Choose at least one background region (e.g., the lumen of an unstained blood vessel) that provides an estimate for background fluorescence that should be subtracted. Note that the number of cells selected trades off against effective cell sampling rate. For example, with our settings and using 5-point RAPS, 100 cells are sampled at 167 Hz, 50 cells at 334 Hz, or 30 cells at 556 Hz.

43. During the pattern scan on each cell continuously integrate the fluorescence signal, interrupting only during the brief transition periods when the laser focus is transiting to the next neuron.

    In our setup we used a five-point pattern and a total signal integration time of 50 µsec/cell (Fig. 2B). Although the 10-mm aperture size of our AODs theoretically supports a point-to-point transition time of 15.4 µsec (sound velocity 650 m/sec), this can be shortened without any measurable effects to 10 µsec (Otsu et al. 2008), in particular when the AOD aperture is underfilled. For frame scanning, an additional pixel dwell time of 2–3 µsec results in an acquisition time of ~800 msec for a 256 × 256-pixel frame.

44. For optimizing the signal-to-noise ratio (SNR) of the fluorescence recordings from neuronal somata, you can either increase the signal integration time per neuron or slightly increase the laser intensity.

45. Start random-access pattern scanning of the neuronal cell population and acquire spontaneous or stimulus-evoked fluorescence signals.

    See Troubleshooting.

46. For each neuron, subtract background fluorescence and convert the raw fluorescence signal to relative percentage fluorescence changes ($\Delta F/F$). From the onsets of the calcium transients, action potential timing can be determined with near-millisecond precision (Grewe et al. 2010). For converting entire fluorescence traces to spike trains, use the "peeling" algorithm described in detail in the original paper (Grewe et al. 2010).

TROUBLESHOOTING

Problem (Step 23): AOD drivers do not work properly (e.g., driving frequencies are not generated).
Solution: Reset the frequency generators of the AOD driver circuit. Check the frequency output with an oscilloscope.

Problem (Step 29): Laser beam power is too low after the objective.
Solution: Look for clipping of the laser beam throughout the microscope. Check proper functioning of the Pockels cell. Check the transmission efficiency of the DCU and the AODs. If transmission is <40%, check the λ/2-wave plates and readjust the laser beam incident angle of the AODs by adjusting the pitch/yaw platform.

Problem (Step 29): Fluorescent beads are distorted (i.e., not round) in the FOV center.
Solution: Recalibrate the DCU by adjusting the incident angle of the compensation prism. Realign the laser beam through the AODs and realign the scan and tube lenses. If installed, realign the cylindrical lens telescope. If the optimal compensation (i.e., round bead) is offset to the side of the FOV's center, increase or reduce the amount of spatial dispersion by changing the incident angle between the laser beam and the compensation prism to ensure optimal compensation in the FOV center.

Problem (Step 29): Astigmatic effects are apparent during axial movement of the focal plane.
Solution: Verify whether the laser beam is centered on all optical components. If a cylindrical telescope is used, check that the lens distance is the exact sum of the focal lengths of the cylindrical lenses. The focusing planes of both lenses must fit properly.

Problem (Step 39): There is no measurable fluorescence signal in any channel.

Solution: Use an IR viewer to see if the laser illuminates the sample. If not, check if and where the alignment of the excitation beam might be off. Make sure all the electronics (AOD drivers and amplifiers, shutters, Pockels cell) are turned on. Check the laser beam alignment. If the laser does illuminate the sample, check all the components of the detection pathway (PMTs, preamplifiers, A/D converters, dichroic mirrors). Try to locate the area of dye injection within the craniotomy. Check the microscope system using fluorescent test samples (e.g., fluorescent beads or pollen grains).

Problem (Step 39): The staining of the neurons is weak and insufficient to measure neuronal activity.

Solution: If dye loading is not optimal, repeat the labeling procedure. Multicell bolus loading critically depends on the quality of the preparation (Garaschuk et al. 2006). If the labeling is sufficient but other factors are limiting (e.g., obstruction of illumination by blood vessels), reduce the scanning speed and increase the cell integration time by raising the number of points scanned on each cell; this will help to maintain a good SNR.

Problem (Step 39): The brightness of the fluorescence signal is inhomogeneous and falls off toward the FOV edges.

Solution: This effect occurs because the AOD deflection efficiency is maximal for the AOD center frequency but changes as a function of the AOD frequency and thus of the scan angle. As a result, the laser illumination is inhomogeneous across the FOV. Because the fast FPGA board controls both AOD driving frequency and the sound wave amplitude (which directly modulates diffraction efficiency), it is possible to compensate for this effect by slightly increasing the sound wave amplitude toward the FOV edges. Try adjusting the AOD sound wave amplitude for each deflection angle until a given transmission efficiency is reached. Perform this calibration for each AOD (x and y) separately.

Problem (Step 45): Motion-induced artifacts during RAPS experiments make recordings difficult.

Solution: During imaging experiments motion artifacts can be caused by tissue pulsation resulting from animal breathing and/or heartbeats. Damp brain tissue pulsation as much as possible by adjusting the animal's posture and by renewing the agarose and coverslip on top of the craniotomy.

DISCUSSION

The characterization of neuronal network dynamics is essential to understanding brain function. Neuronal networks process incoming information as coordinated spike sequences on a millisecond-to-second timescale. Investigation of these activity patterns requires fast readout methods, which in the future will need to be combined with unambiguous identification of neuronal cell types, cell positions, and the functional connectivity within the network organization. Although electrical recordings provide excellent temporal resolution and can reveal spike trains in widely dispersed neuronal populations (Buzsáki 2004), they cannot comprehensively resolve activity patterns in the local microcircuits. The alternative is high-resolution optical imaging, which permits population measurements from many well-identified neurons (for review, see Grewe and Helmchen 2009). In particular, two-photon laser scanning microscopy enables imaging to a depth of several hundred micrometers in optically thick, light-scattering tissue in vivo (for review, see Helmchen and Denk 2005; Kerr and Denk 2008). However, using frame scanning with mechanical scan mirrors in a standard two-photon microscope, the temporal resolution of population measurements has been limited maximally to 15–30 Hz (Kerr et al. 2005; Rochefort et al. 2009). Hence, in vivo optical recordings of network dynamics on the millisecond timescale have not been possible so far.

One alternative to mechanical laser scanning is scanning with acousto-optical deflectors (AODs) (Reddy and Saggau 2011). AOD scanners enable transitions of the laser focus within several micro-

 Cite this protocol as *Cold Spring Harb Protoc*; doi:10.1101/pdb.prot081778

seconds between any two positions in the scanning area. Such fast transitions avoid the waste of scanning time on background regions and enable random-access scanning from preselected points of interest only (e.g., neurons). AODs are, however, limited by their low laser diffraction efficiency (~55% transmission for an *x*–*y* pair of AODs) and the large optical dispersion of the acousto-optic crystal, which causes laser pulse broadening and spatial deformation of the laser focus. Using relatively long laser pulses (0.5–1.8 psec) can minimize dispersive effects (Iyer et al. 2006; Otsu et al. 2008; Reddy et al. 2008), although this reduces two-photon fluorescence excitation. Alternatively, adding diffractive elements can compensate for the dispersion (Zeng et al. 2006, 2007; Kremer et al. 2008; Kirkby et al. 2010). For a broader discussion of fast-scanning and scanless laser microscopes, see Bansal and Saggau (2011), Liebling (2011), Nikolenko et al. (2011), Oron and Silberberg (2011), and Reddy and Saggau (2011).

Several AOD-based two-photon microscopes have been applied to calcium imaging from neuronal dendrites in brain slices (Iyer et al. 2006; Otsu et al. 2008; Reddy et al. 2008), but their application to measure network dynamics in the intact brain has been pending. The high-speed AOD-based two-photon microscope optimized for in vivo imaging applications (Grewe et al. 2010) now provides a means for recording neuronal activity in living animals.

Imaging Setup

We first provide a list of the hardware components that are necessary to build the microscope and then discuss several design considerations.

Laser and Accessories

Beam expander, variable (S6ASS2075, Sill Optics)
Infrared (IR) viewer, miniature, 350–1700 nm (IRV1-1700, Newport Corporation)
Laser intensity modulator (i.e., Pockels cell; #M350-80, Conoptics)
Laser system, Ti:sapphire, capable of producing an average power >2.8 W at 850 nm (e.g., Chameleon Ultra II, Coherent, Inc.)
Mirror mounts, kinematic, metric (KMS/M, Thorlabs, Inc.)
Mirrors, broadband, dielectric, 750–1100-nm, 1-in and 2-in-diameter (BB1-E03 and BB2-E03, respectively, Thorlabs, Inc.)
Power and energy meter console (PM100D, Thorlabs, Inc.)
Thermal power sensor, C-Series (S350C, Thorlabs, Inc.)

Microscope Stand

Optical table, equipped with four stabilizers (RS2000 series and S-2000, respectively, Newport Corporation)
Precision linear stage (i.e., *z* stage; model PMT 160-DC, Feinmess Dresden GmbH)
Rail system (e.g., Profile X95-640 column, baseplate, and six to eight clamps [LINOS Photonics])
x–*y* stage, compact, motorized (KT310, Feinmess Dresden GmbH)
x–*y*–*z* stage controller (Galil)

Scanning Apparatus and DCU

AOD-alignment platform (e.g., pitch and yaw platform w/micrometers; PY003, Thorlabs, Inc.)
AODs, high-resolution, large-scan-angle (DTSXY-A12-850, AA Opto-Electronic)
Compensation prism, N-SF11, uncoated, apex angle 60° (e.g., equilateral dispersive prism; Thorlabs, Inc.) (Alternatively, use an uncoated custom prism (N-SF66, apex angle 60°.))
Computer, equipped with quad-core processor (e.g., HP Compaq dc7900, Hewlett Packard)
Frequency generators (two) (e.g., CMOS 300 MSPS Complete DDS digital synthesizer; AD9852, Analog Devices)

Half-wave (λ/2) plate modules, zeroth-order (two) (RZBH-850, Thorlabs, Inc.)
Lenses, cylindrical telescope, achromatic, N-BK7, focal lengths $f_1 = 100$ mm and $f_2 = 50$ mm (Thorlabs, Inc.) (for use with N-SF11 prism [Thorlabs, Inc.] only)
Power amplifiers (two) (AMPA-B-36, AA Opto-Electronic)
Rotation mount, prism, high-precision (PR01/M, Thorlabs, Inc.)
Rotation mounts, λ/2 plate (two) (e.g., rotation mount for 25.4-mm-diameter optics; RSP1/M, Thorlabs, Inc.)
Scan control board, field-programmable gate array (PXI-7813R, National Instruments)
Scan lens, achromatic, near-infrared coating, $f_{SL} = 300$ mm (Thorlabs, Inc.)
Scan software, custom, written in LabVIEW 2009 (National Instruments)
Tube lens, achromatic, $f_{TL} = 180$ mm (Olympus)

Detection Pathway

Analog/digital (A/D) converter, 40-MHz (custom design, CSEM)
Beam splitter, two-photon (cold light mirror KS 93/45°, LINOS Photonics GmbH)
Data acquisition board, FPGA (NI PXI-7813R, National Instruments)
Dichroic mirror, DC green (LINOS Photonics GmbH)
Emission filter, green (HQ 535/50, Chroma Technology)
Emission filter, red (720SP, AHF Tübingen)
Microscope objectives (40× LUMPlanFl/IR, numerical aperture (NA) 0.8; 10× UPLFLN 10 × 2, NA 0.3 [Olympus]) (The 10× objective is used for large-field overviews of preparations.)
Photomultiplier tube (PMT) preamplifier (XPG-ADC-PREAMP, Sigmann-Elektronik)
PMTs (e.g., R6357, Hamamatsu)

Design Considerations

The AOD microscope described here was designed as a "fixed-stage" microscope that can be moved over the sample. This design provides a large space below the objective lens and supports simultaneous stable electrophysiological recordings during in vivo imaging experiments using a table-mounted manipulator. The complete microscope is built around an X95 aluminum column mounted on a motorized *x*–*y* stage (Fig. 1A). Several important issues must be taken into account. The AOD specifications, together with the choice of objective and lenses, determine the image resolution and the FOV size. Because the maximal AOD scan angle (θ) is limited (typically 47 mrad), the number of resolvable spots (N) is limited too, depending on the laser beam size at the AOD aperture (Fig. 1B). For a Gaussian laser beam of full $1/e^2$ width D and wavelength λ, $N = \pi/4 \times \theta \times D/\lambda$ (Kremer et al. 2008). If one is interested in the best possible optical resolution, the laser beam should be expanded to fill the AOD aperture (to maximize N) and the FOV size should be maximally $S \times N$, where S is the diffraction-limited spatial resolution as determined by the effective NA of the microscope objective. If one is rather interested in a large FOV (e.g., to functionally image neuronal populations), one has to accept that the image resolution may be limited by the AOD pointing precision (to ~1 µm in the FOV center in our setup; Grewe et al. 2010). To obtain a certain FOV size, choose a combination of scan and tube lens for a particular microscope objective (i.e., first choose the desired FOV size, then the objective, and finally the scan lens). The tube lens should be selected so that objective magnification is maintained (e.g., $f_{TL} = 180$ mm for Olympus or Nikon objectives). Because the combination of the scan and tube lenses acts as a telescope—thus changing the laser beam diameter—the corresponding demagnification (or magnification) should match the factor required to image the laser beam at the AOD aperture into the objective's back aperture. The system described here produces a maximum FOV of 305 µm × 305 µm with a 40× objective (scan lens–tube lens telescope demagnification of 0.6).

The second key optical component is the DCU (Fig. 1C). A single-prism compensation approach (Zeng et al. 2006) was modified and optimized for laser beam transmission and scan resolution over a

Cite this protocol as *Cold Spring Harb Protoc*; doi:10.1101/pdb.prot081778

large FOV. Two λ/2-wave plates before the prism and the AODs, respectively, turn laser beam polarization along the pathway and thereby maximize transmission through the prism (85%) and the AOD pair (55%). Overall, 45% of the incoming light is transmitted by the DCU and AOD scanners. With a standard SF11 prism the beam path is not symmetrical through the prism, which makes the beam elliptical after the prism. This effect can be corrected, however, by using a cylindrical telescope in front of the prism, restoring a nearly round laser beam profile at the AOD aperture (Grewe et al. 2010). Alternatively, the SF11 prism can be replaced with a custom N-SF66 prism for which the beam path is symmetric, eliminating the need for the cylindrical telescope.

Example of Application

To directly show RAPS recording we measured fluorescence traces from a neuronal population of 53 cells in mouse barrel cortex at a 314-Hz cell sampling rate (Fig. 2C–E). Repetitive stimulation of the contralateral whiskers evoked calcium transients with rapid onsets and $\Delta F/F$ amplitudes in the range of 5%–20% (Fig. 2D). With a peeling algorithm for the automated spike reconstruction algorithm (Grewe et al. 2010), we were able to extract a model of action potential–evoked calcium transients that closely followed the experimental data and thereby provide an estimate of the underlying spike train. The accuracy of spike time reconstruction was verified using simultaneous juxtacellular recordings from single neurons together with the population RAPS measurement and analyzing the time difference Δt between the spike times predicted from the calcium transient onsets and the true spike times as revealed by juxtacellular recording (Fig. 2E). This analysis showed that the high cell sampling rates allowed a reliable and precise action potential reconstruction from the optical recordings with near-millisecond precision (Grewe et al. 2010).

Future Directions

By scanning small point patterns on each individual neuron, the RAPS mode enables measurements with high SNR and enables a post hoc reconstruction of spike times with near-millisecond accuracy (Grewe et al. 2010). The imaging depth of the AOD microscope is sufficient to visualize neuronal activity of L2/3 neurons in mouse neocortex down to 300 μm below the pia. At present it will be difficult to make recordings at much greater depths because of the slightly reduced spatial resolution of the AOD system and laser power limitations. Compared with in vivo imaging studies using standard galvanometric scan mirrors (1–30-Hz frame rate; Kerr et al. 2005; Ohki et al. 2005; Sato et al. 2007; Rochefort et al. 2009), the AOD-based imaging approach provides up to a 500-Hz cell sampling rate on populations of comparable size, hence gaining a factor of 16–500 in temporal resolution. Although user-defined line-scanning approaches can also be used to increase sampling speed (Göbel et al. 2007; Lillis et al. 2008; Rothschild et al. 2010), it is unclear whether they can reach a comparable SNR as the AOD-based RAPS measurements.

All fluorescence traces shown in Figure 2 are raw traces without any filtering. The excellent SNR at the high sampling rates is explained by the rather long dwell times per cell and the efficient fluorescence collection. AOD-based scanning thus opens new ways to measure spatiotemporal spiking dynamics in the living brain across neuronal populations of 10–100 cells with a few milliseconds resolution. We expect this method to facilitate in vivo imaging studies, for which a high temporal resolution is essential. This in particular concerns questions related to spike timing within neuronal populations (e.g., phase relationships of spiking activity relative to global oscillations) or to circuit plasticity, where relative spike timing is crucial for modulation of synaptic strength.

There are several promising future directions for AOD-based microscopy. First, although our in vivo measurements so far were restricted to a single focal plane, they should be extendable to 3D by using either mechanical z scanning in combination with AOD-based lateral scanning (Göbel et al. 2007) or chirped acoustic waves in a series of AODs (Vučinić and Sejnowski 2007; Reddy et al. 2008; Kirkby et al. 2010). Extending the method volumetrically would allow the measurement of neural dynamics in local 3D networks. Second, the combination of high-speed AOD-based imaging with genetically encoded calcium indicators (Mank et al. 2008; Wallace et al. 2008; Tian et al. 2009; Lütcke

et al. 2010) should allow for repeated long-term functional interrogation of neuronal networks. A third goal is to perform high-speed AOD-based calcium imaging in awake animals (Dombeck et al. 2007; Greenberg and Kerr 2009). This faces particular challenges because the AOD-RAPS mode is especially sensitive to motion artifacts, which are expected under awake conditions. Finally, improvements in algorithms for inferring neuronal spiking from noisy fluorescence traces (Kerr et al. 2007; Vogelstein et al. 2009; Grewe et al. 2010) are possible and could increase the reliability and precision of spike train reconstruction. In summary, the combination of fast optical recording with AODs, a high SNR, and a reliable automated spike reconstruction will facilitate the spatiotemporal analysis of neuronal population activity on the level of local microcircuits and thus help to reveal fundamental aspects of neural coding.

RECIPE

Normal Rat Ringer's Solution

Reagent	Concentration	Amount for 1 L	Amount for 2 L
NaCl	135 mM	7.88 g	15.76 g
KCl	5.4 mM	0.40 g	0.80 g
$MgCl_2 \cdot 6H_2O$	1 mM	0.204 g	0.408 g
$CaCl_2 \cdot 2H_2O$	1.8 mM	0.265 g	0.530 g
HEPES	5 mM	1.19 g	2.38 g

Adjust pH to 7.2 with NaOH. Final osmolarity is ~290 mOsm. This solution can be stored at 4°C for 1 mo.

ACKNOWLEDGMENTS

This work was supported by a Forschungskredit of the University of Zurich (BG), and by grants to FH from the Swiss National Science Foundation (Grant 3100A0-114624), the EU-FP7 program (SPACE-BRAIN project 200873), and the Swiss SystemsX.ch initiative (project 2008/2011-Neurochoice).

REFERENCES

Bansal V, Saggau P. 2011. Digital micromirror devices: Principles and applications in imaging. In *Imaging: A laboratory manual* (ed. Yuste R), pp. 839–848. Cold Spring Harbor Laboratory Press, Cold Spring Harbor, NY.

Buzsáki G. 2004. Large-scale recording of neuronal ensembles. *Nat Neurosci* **7:** 446–451.

Dombeck DA, Khabbaz AN, Collman F, Adelman TL, Tank DW. 2007. Imaging large-scale neural activity with cellular resolution in awake, mobile mice. *Neuron* **56:** 43–57.

Garaschuk O, Konnerth A. 2010. In vivo two-photon calcium imaging using multicell bolus loading. *Cold Spring Harbor Protoc* doi:10.1101/pdb.prot5482.

Garaschuk O, Milos R-I, Konnerth A. 2006. Targeted bulk-loading of fluorescent indicators for two-photon brain imaging in vivo. *Nat Protoc* **1:** 380–386.

Göbel W, Kampa BM, Helmchen F. 2007. Imaging cellular network dynamics in three dimensions using fast 3D laser scanning. *Nat Methods* **4:** 73–79.

Greenberg DS, Kerr JN. 2009. Automated correction of fast motion artifacts for two-photon imaging of awake animals. *J Neurosci Methods* **176:** 1–15.

Grewe BF, Helmchen F. 2009. Optical probing of neuronal ensemble activity. *Curr Opin Neurobiol* **19:** 520–529.

Grewe BF, Langer D, Kasper H, Kampa BM, Helmchen F. 2010. High-speed in vivo calcium imaging reveals neuronal network activity with near-millisecond precision. *Nat Methods* **7:** 399–405.

Helmchen F, Denk W. 2005. Deep tissue two-photon microscopy. *Nat Methods* **2:** 932–940.

Iyer V, Hoogland TM, Saggau P. 2006. Fast functional imaging of single neurons using random-access multiphoton (RAMP) microscopy. *J Neurophysiol* **95:** 535–545.

Kerr JND, Denk W. 2008. Imaging in vivo: Watching the brain in action. *Nat Rev Neurosci* **9:** 195–205.

Kerr JND, Greenberg D, Helmchen F. 2005. Imaging input and output of neocortical networks in vivo. *Proc Natl Acad Sci* **102:** 14063–14068.

Kerr JND, de Kock CPJ, Greenberg DS, Bruno RM, Sakmann B, Helmchen F. 2007. Spatial organization of neuronal population responses in layer 2/3 of rat barrel cortex. *J Neurosci* **27:** 13316–13328.

Kirkby PA, Srinivas Nadella KM, Silver RA. 2010. A compact acousto-optic lens for 2D and 3D femtosecond based 2-photon microscopy. *Opt Express* **18:** 13721–13745.

Kremer Y, Léger J-F, Lapole R, Honnorat N, Candela Y, Dieudonné S, Bourdieu L. 2008. A spatio-temporally compensated acousto-optic scanner for two-photon microscopy providing large field of view. *Opt Express* **16:** 10066–10076.

Liebling M. 2011. Imaging the dynamics of biological processes via fast confocal microscopy and image processing. In *Imaging: A laboratory manual* (ed. Yuste R), pp. 823–830. Cold Spring Harbor Laboratory Press, Cold Spring Harbor, NY.

Lillis KP, Eng A, White JA, Mertz J. 2008. Two-photon imaging of spatially extended neuronal network dynamics with high temporal resolution. *J Neurosci Methods* **172:** 178–184.

Lütcke H, Murayama M, Hahn T, Margolis DJ, Astori S, zum Alten Borgloh SM, Göbel W, Yang Y, Tang W, Kügler S, et al. 2010. Optical recording of neuronal activity with a genetically-encoded calcium indicator in anesthetized and freely moving mice. *Front Neural Circuits* **4:** 9.

Mank M, Santos AF, Direnberger S, Mrsic-Flogel TD, Hofer SB, Stein V, Hendel T, Reiff DF, Levelt C, Borst A, et al. 2008. A genetically encoded calcium indicator for chronic in vivo two-photon imaging. *Nat Methods* **5:** 805–811.

Nikolenko V, Peterka DS, Araya R, Woodruff A, Yuste R. 2011. Spatial light modulator microscopy. In *Imaging: A laboratory manual* (ed. Yuste R), pp. 849–860. Cold Spring Harbor Laboratory Press, Cold Spring Harbor, NY.

Nimmerjahn A, Helmchen F. 2012. In vivo labeling of cortical astrocytes with sulforhodamine 101 (SR101). *Cold Spring Harb Protoc* doi:10.1101/pdb.prot068155.

Nimmerjahn A, Kirchhoff F, Kerr JND, Helmchen F. 2004. Sulforhodamine 101 as a specific marker of astroglia in the neocortex in vivo. *Nat Methods* **1:** 31–37.

Ohki K, Chung S, Ch'ng YH, Kara P, Reid RC. 2005. Functional imaging with cellular resolution reveals precise micro-architecture in visual cortex. *Nature* **433:** 597–603.

Oron D, Silberberg Y. 2011. Temporal focusing microscopy. In *Imaging: A laboratory manual* (ed. Yuste R), pp. 861–868. Cold Spring Harbor Laboratory Press, Cold Spring Harbor, NY.

Otsu Y, Bormuth V, Wong J, Mathieu B, Dugué GP, Feltz A, Dieudonné S. 2008. Optical monitoring of neuronal activity at high frame rate with a digital random-access multiphoton (RAMP) microscope. *J Neurosci Methods* **173:** 259–270.

Reddy GD, Saggau P. 2011. High-speed two-photon imaging. In *Imaging: A laboratory manual* (ed. Yuste R), pp. 831–839. Cold Spring Harbor Laboratory Press, Cold Spring Harbor, NY.

Reddy GD, Kelleher K, Fink R, Saggau P. 2008. Three-dimensional random access multiphoton microscopy for functional imaging of neuronal activity. *Nat Neurosci* **11:** 713–720.

Rochefort NL, Garaschuk O, Milos R-I, Narushima M, Marandi N, Pichler B, Kovalchuk Y, Konnerth A. 2009. Sparsification of neuronal activity in the visual cortex at eye-opening. *Proc Natl Acad Sci* **106:** 15049–15054.

Rothschild G, Nelken I, Mizrahi A. 2010. Functional organization and population dynamics in the mouse primary auditory cortex. *Nat Neurosci* **13:** 353–360.

Sato TR, Gray NW, Mainen ZF, Svoboda K. 2007. The functional microarchitecture of the mouse barrel cortex. *PLoS Biol* **5:** e189.

Stosiek C, Garaschuk O, Holthoff K, Konnerth A. 2003. In vivo two-photon calcium imaging of neuronal networks. *Proc Natl Acad Sci* **100:** 7319–7324.

Tian L, Hires SA, Mao T, Huber D, Chiappe ME, Chalasani SH, Petreanu L, Akerboom J, McKinney SA, Schreiter ER, et al. 2009. Imaging neural activity in worms, flies and mice with improved GCaMP calcium indicators. *Nat Methods* **6:** 875–881.

Vogelstein JT, Watson BO, Packer AM, Yuste R, Jedynak B, Paninski L. 2009. Spike inference from calcium imaging using sequential Monte Carlo methods. *Biophys J* **97:** 636–655.

Vučinić D, Sejnowski TJ. 2007. A compact multiphoton 3D imaging system for recording fast neuronal activity. *PLoS ONE* **2:** e699.

Wallace DJ, zum Alten Borgloh SM, Astori S, Yang Y, Bausen M, Kügler S, Palmer AE, Tsien RY, Sprengel R, Kerr JND, et al. 2008. Single-spike detection in vitro and in vivo with a genetic Ca^{2+} sensor. *Nat Methods* **5:** 797–804.

Zeng S, Lv X, Zhan C, Chen WR, Xiong W, Jacques SL, Luo Q. 2006. Simultaneous compensation for spatial and temporal dispersion of acousto-optical deflectors for two-dimensional scanning with a single prism. *Opt Lett* **31:** 1091–1093.

Zeng S, Lv X, Bi K, Zhan C, Li D, Chen WR, Xiong W, Jacques SL, Luo Q. 2007. Analysis of the dispersion compensation of acousto-optic deflectors used for multiphoton imaging. *J Biomed Opt* **12:** 024015.

High-Speed Two-Photon Calcium Imaging of Neuronal Population Activity Using Acousto-Optic Deflectors

Benjamin F. Grewe and Fritjof Helmchen

Cold Spring Harb Protoc; doi: 10.1101/pdb.prot081778